

## Deflection and crack analysis of single span concrete beams reinforced with basalt fiber reinforced polymer bars

Abel A. Belay<sup>1\*</sup> , Marta Kosior-Kazberuk<sup>1</sup> , Julita Krassowska<sup>1</sup> 

<sup>1</sup> Department of Building Structures and Structural Mechanics, Białystok University of Technology, Wiejska 45A, Białystok, Poland

\* Corresponding author's e-mail: [abel.belay@sd.pb.edu.pl](mailto:abel.belay@sd.pb.edu.pl)

### ABSTRACT

The study investigated the deflection, cracking behaviour and load bearing capacity of single span concrete beams reinforced with basalt fiber reinforced polymer (BFRP) bars and steel-reinforced concrete beams with similar reinforcement ratios, under similar loading and support conditions. The experiment focused on key parameters, such as ultimate load-bearing capacity, midspan deflection, crack patterns and failure modes of the beam cross-section. Four beams (80 × 120 × 1100 mm) were tested—two reinforced with 6 mm steel bars and two with 6 mm BFRP bars. The test results revealed that the concrete beams reinforced with BFRP bars showed 35% higher load carrying capacity but also greater deflection and earlier cracking than steel reinforced concrete beams. Theoretical values were calculated based on different scholars' assumptions and compared with experimental results to validate performance.

**Keywords:** BFRP bars, FRP, steel bars, concrete beam.

### INTRODUCTION

Concrete is typically reinforced with steel bars in the regions expected to experience tension. Steel is widely used in the construction industry for reinforcing structural elements due to its exceptional tensile strength [1]. It is the perfect material for reinforcing concrete buildings because of its capacity to endure high strain stresses. Despite its widespread use, steel reinforcement has several drawbacks that warrant consideration [2]. The vulnerability of steel reinforcement to corrosion is a significant drawback. Over time, steel can corrode due to the exposure to oxygen and moisture which affects the structural integrity of the material. Certain settings, such as coastal places with high quantities of seawater or areas with high humidity, might speed up the corrosion process. Corrosion not only weakens the steel reinforcement but also leads to cracking and deterioration in the surrounding concrete, ultimately compromising

the overall structural stability. The comparatively heavy weight of steel reinforcing is another disadvantage. Steel is a dense material, and when utilized in large amounts, it significantly increases the weight of the construction as a whole. This can pose challenges during installation, transportation, and construction.

In recent years, researchers have turned their attention to fiber reinforced polymer (FRP) as a viable alternative to steel reinforcement [3–5]. FRP provides multiple benefits compared to steel, such as a superior strength-to-weight ratio, excellent corrosion resistance, and enhanced durability in challenging environments [6–9]. FRP reinforcements are also significantly lighter than steel, simplifying installation and reducing transportation costs. Furthermore, the tensile strength of FRP reinforcements can surpass that of steel by up to 10 times, while its weight is only approximately 25% of that of steel [10–12]. Consequently, FRP has emerged as a compelling choice for the infrastructure projects that prioritize durability and longevity [13].

The research aimed to investigate the stiffness of concrete beams reinforced with BFRP bars. From previous studies, BFRP bar reinforced concrete beams exhibit greater ultimate load carrying capacities compared to steel reinforced concrete beams. For instance, Urbanski et al. [14] reported that the concrete beams reinforced with BFRP bars exhibited a greater ultimate load-carrying capacity than those reinforced with steel. This increase in capacity highlights the superior tensile strength of FRP reinforcement, as supported by ACI Committee 440 [10].

Although BFRP bars offer several advantages, research [15, 16] has highlighted significantly greater deflections in BFRP-reinforced concrete beams compared to those reinforced with steel. This increased deflection is attributed to the lower modulus of elasticity of BFRP bars relative to steel bars [17]. Additionally, Kosior-Kazberuk et al. [16] observed that the concrete beams reinforced with BFRP bars exhibited considerably more deformation than steel-reinforced beams. During the initial loading phase, the BFRP-reinforced beams deflected approximately 40% more than their steel-reinforced counterparts. As the load intensified, the disparity became even more evident, with the BFRP-reinforced beams ultimately bending twice as much as those with steel reinforcement. With the first crack appearing when the load reached 10% of the beam's ultimate load capacity, Krassowska et al. [15] observed that the BFRP-reinforced beams developed a larger number of cracks with greater widths. Still, the flexural capacity of beams with FRP reinforcement exhibited appreciable increases. Important understanding of the failure modes of FRP-reinforced beams was given by Ashour [18]. Still, ACI Committee 440 [10] noted somewhat low transverse shear resistance of FRP materials. Urbanski et al. [14] highlighted the need for further research, as the basalt bar-reinforced beams exhibited crack widths three to four times larger than those in conventional concrete beams. Developing a detailed model to precisely estimate the shear capacity of FRP-reinforced concrete beams would improve the understanding and help ensure the structural reliability of FRP in construction.

Recent studies have continued to explore the mechanical and structural behavior of FRP-reinforced concrete beams. Zhang et al. [19] reviewed the short-term mechanical properties of FRP bars and FRP-reinforced beams, emphasizing their relevance in practical applications. Li et al. [20]

examined the dynamic torsional performance of geometrically similar BFRP-reinforced beams, providing insights into failure modes under complex loading. Kumar et al. [21] conducted experimental investigations on how fiber type and surface characteristics of FRP bars influence beam behavior, contributing to material optimization in beam design.

While these studies have contributed to understanding the mechanical and material properties of BFRP bars, they often fall short in connecting experimental results with a broad comparison of theoretical models, particularly regarding stiffness and deflection predictions. Furthermore, many earlier works have not directly compared BFRP and steel reinforcement under identical conditions, using both laboratory testing and model-based analysis.

This study aimed to bridge that gap by evaluating the performance of the concrete beams reinforced with BFRP bars under static loads and comparing them to the steel reinforced concrete beams with similar reinforcement ratios. Key parameters such as crack patterns, deflections and failure modes were examined. While many previous studies have primarily focused on the material properties of BFRP bars, this research goes a step further by comparing the structural behavior of BFRP bar reinforced concrete beams with that of conventional steel reinforced concrete beams. Moreover, the study provides a comparative analysis of deflection and crack width results using various established models from the literature. This dual approach not only enhances the understanding of the structural performance of a BFRP bar but also offers valuable insights for refining and improving current stiffness and deflection prediction models. The findings contribute to the development of more accurate design guidelines for the BFRP bar-reinforced concrete elements, which hold significant promise for future construction applications.

## METHODOLOGY

### Test specimens and material characteristics

The concrete mix ratio for sample preparation was shown in Table 1. The cement used for the experiment was CEM I 42.5R Portland cement. Different strength tests were used to evaluate the concrete strength characteristics in order to

**Table 1.** Concrete mix ratio

Water-to-cement ratio	Cement [kg/m <sup>3</sup> ]	Water [kg/m <sup>3</sup> ]	Sand ≤ 2 mm [kg/m <sup>3</sup> ]	Gravel 2–16 mm [kg/m <sup>3</sup> ]	Superplasticizer [kg/m <sup>3</sup> ]
0.5	320	160	732	1203	3.2

ensure that it met the required standards. Compressive strength tests were conducted based on EN 12390-3:2009 [22], while concrete tensile strength was evaluated following EN 12390-5:2019 [23]. Additionally, cylindrical samples were used to measure the modulus of elasticity according to EN 12390-13:2013 [24]. The test results, including the average values, standard deviations, and coefficients of variation, are presented in Table 2.

Both the steel and BFRP bars for the beam samples were acquired locally. As illustrated in Figure 1, helical basalt fiber strands were applied to the BFRP bar surfaces to improve bonding performance. As shown in Figure 2, 6 mm diameter S-500 steel bars were used, with a characteristic yield strength of 500 MPa, an approximate tensile strength of 550 MPa and 200 GPa modulus of elasticity and 6 mm diameter BFRP bars with a tensile strength of 1180 MPa, 47.6 GPa modulus of elasticity for longitudinal reinforcement.

**Test procedure**

The study conducted an experimental program that focused on a number of important characteristics in order to better understand their ability to BFRP bars work in concrete beams. These included

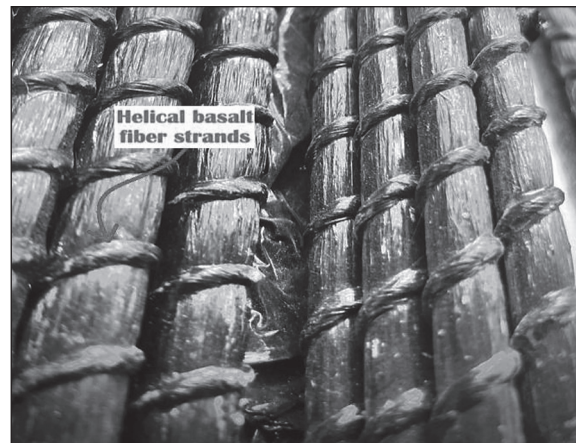


**Figure 1.** BFRP bars with helical basalt fiber strands

**Table 2.** Mechanical properties of concrete

Test parameter	Average value ± SD	CV (%)
Cube compressive strength (MPa)	59.66 ± 1.98	3.32
Tensile strength (MPa)	3.06 ± 0.05	1.63
Modulus of elasticity (GPa)	33.53 ± 0.39	1.16

**Note:** SD – standard deviation; CV – coefficient of variation.

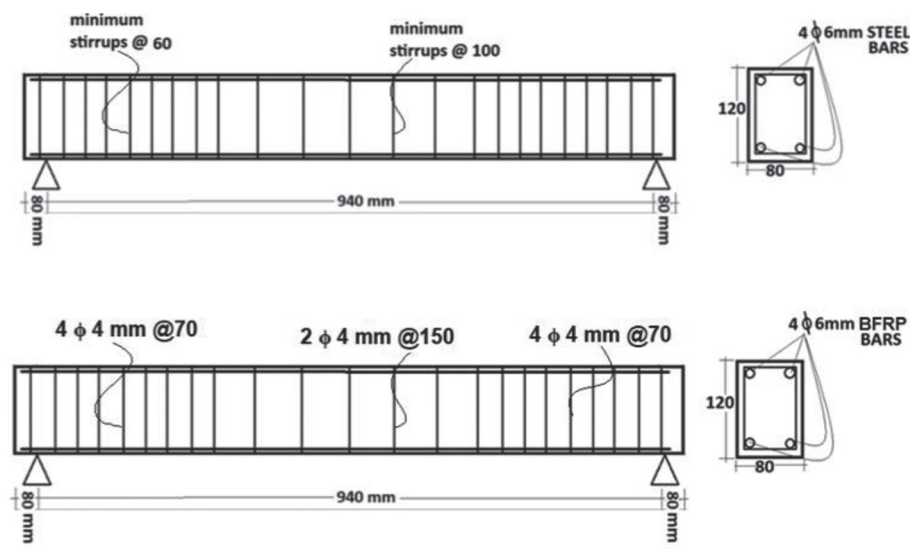


**Figure 2.** Reinforcement details of specimens

the ultimate load-bearing capacity, the beams failure modes, cracking patterns, and the maximum deflection. Four concrete beams with dimensions of  $80 \times 120 \times 1100$  mm were used in the experiment. It included two steel reinforced concrete beams (STL-1 and STL-2), along with two BFRP bar reinforced concrete beams, (BFP-1 and BFP-2). The concrete beams reinforced with BFRP bars were developed following the standards by ACI Committee 440 [10]. The main goal of the test, following ACI Committee 440 [10] guidelines, was to evaluate how effectively BFRP bars enhance the stiffness and load capacity of concrete beams. Each beam was set up with simple supports, and point loads were applied at one-third of the beam length from each end, as depicted in Figure 3.

During the testing process, the ultimate bending capacity of each element was recorded along with measurements of midspan deformations, maximum deflections, and the formation and progression of cracks and failure modes. Before starting the tests, an initial preload of 0 kN was applied to the beams. The load was then progressively increased in 2 kN increments every 30 seconds, remained constant for around 30 seconds at each level to enable data recording. The load was applied via a hydraulic cylinder, controlled through the control panel of the PZA machine. Inductive sensors from the Megatron-Munich return spring, placed at the midspan of the specimen, were used to measure deflection. Crack widths were documented at each load increment based on the captured images.

## RESULTS

During the stiffness test, the following relevant data were recorded: the load at which the initial

crack was observed, the ultimate load before failure, (as outlined in Table 1), the number and pattern of cracks at each 2 kN load increment, and the deflection at each load phase. The subsequent sections analyze and interpret the collected data (Table 3).

### Ultimate load bearing capacity

The load bearing capacity of the entire beams was observed, recorded, and graphically illustrated in Figure 4.

The load bearing capacity of the beams reinforced with BFRP bars was higher than that of the beams reinforced with steel. Although steel reinforced concrete beams could sustain higher loads before the initial cracking appeared, they failed more rapidly. In contrast, the BFRP bar-reinforced concrete beams began to crack sooner than the steel reinforced beams but ultimately exhibited higher load bearing capacity. The average ultimate load bearing capacity of the concrete beams reinforced with BFRP bars was 35% greater than that of the steel reinforced beams. This improvement is due to the higher tensile strength of BFRP bars compared to steel.

### Crack patterns and mode of failure

Overall, all beams exhibited similar crack patterns prior to failure. The initial crack consistently formed near the mid-span of the beam in a vertical orientation, with its occurrence varying based on the reinforcement type and concrete strength, as illustrated in Figure 5. With increasing load, additional flexural cracks emerged in both the mid-span and shear span regions. Existing cracks widened and deepened significantly, especially in the BFRP-reinforced concrete beams (Figure 5c and 5d), due to the lower modulus of elasticity of

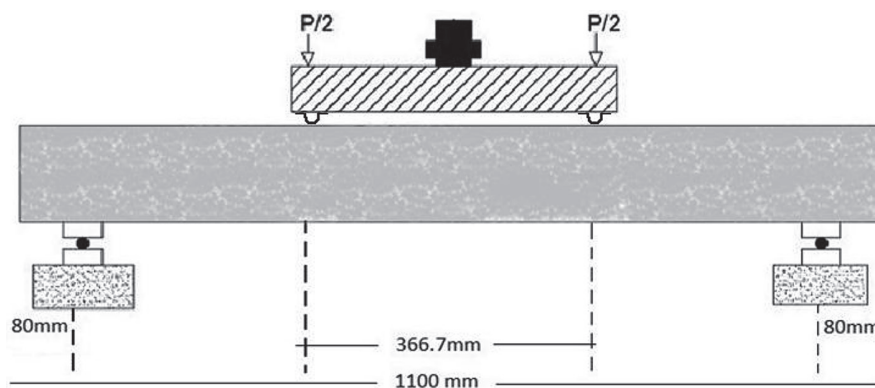
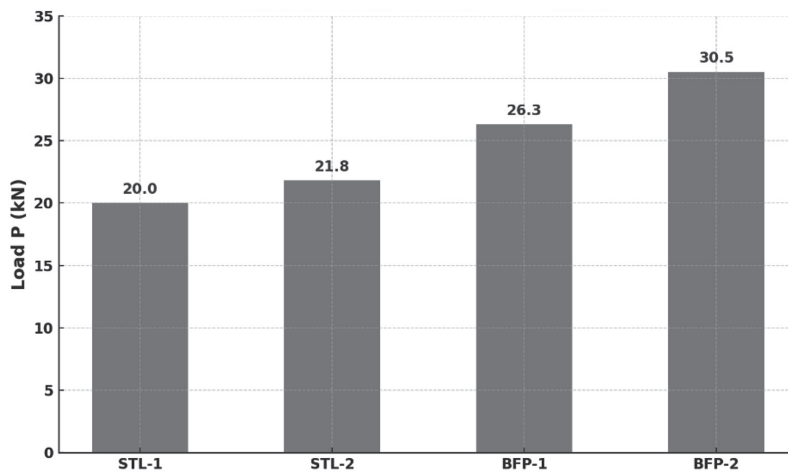


Figure 3. Test setup

**Table 3.** Test results

Beam notations	b (mm)	D (mm)	Longitudinal STEEL bars				$f_{cu}$ (N/mm <sup>2</sup> )	$P_{cr}$ (kN)	$P$ (kN)	$\rho_b$
			No. $\phi$ diameter (mm)	$\rho_s$ (%)	$E$ (kN/mm <sup>2</sup> )	$f_{fu}$ (N/mm <sup>2</sup> )				
STL-1	80	120	4 $\phi 6$	1.76	210	315	56.66	8	20	0.09
STL-2	80	120	4 $\phi 6$	1.76	210	315		10	21.8	0.09
			Longitudinal BFRP bars							
			No. $\phi$ diameter (mm)	$\rho_f$ (%)	$E_f$ (kN/mm <sup>2</sup> )	$f_{fu}$ (N/mm <sup>2</sup> )				
BFP-1	80	120	4 $\phi 6$	1.76	47.6	1180	59.66	2	26.3	0.004
BFP-2	80	120	4 $\phi 6$	1.76	47.6	1180		2	30.5	0.004

**Note:**  $D$  – the overall depth of the test specimens;  $\rho_s$  and  $\rho_f$  – the reinforcement ratios for steel and BFRP bars respectively, determined as  $A_f/bd$ ;  $A_f$  – the cross-sectional area of the reinforcement bars;  $b$  and  $d$  – the width and effective depth of the test specimens respectively.  $\rho_b$  – the balanced reinforcement ratio of FRP bars.  $E_f$  and  $f_{fu}$  – the modulus of elasticity and the tensile rupture strength of the reinforcement bars, respectively, while  $f_{cu}$  is the cube compressive strength of the concrete.  $P_{cr}$  – the total load at which the first visible crack appears, and  $P$  – represents the total failure load. When the reinforcement ratio ( $\rho_f$ ) is lower than the balanced ratio ( $\rho_b$ ), FRP bars are prone to rupture ( $\rho_f < \rho_b$ ). On the other hand, if  $\rho_f$  surpasses  $\rho_b$ , the failure mechanism is governed by concrete crushing.



**Figure 4.** Ultimate load-bearing capacity of the beam specimens

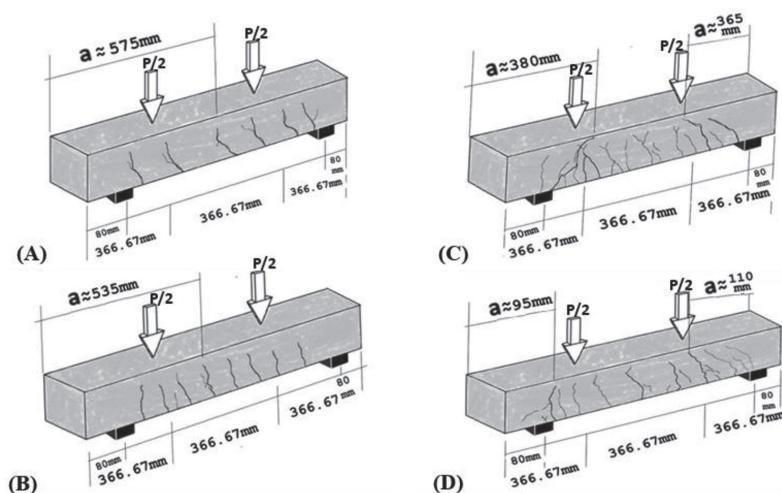


**Figure 5.** Failure of specimens due to concrete crushing (A) STL-1, (B) STL-2, (C) BFP-1, (D) BFP-2. P denotes the applied load, and a represents the distance between the maximum crack and the edge of the concrete beam



Figure 6. Actual image of concrete sample BFP-1

BFRP bars relative to their tensile strength. The oblique and horizontal cracking observed at the supports of BFRP-reinforced concrete beams, as shown in Figure 6 – a close-up image of the crack on sample BFP-1 – clearly indicates shear failure in addition to bending failure.

Theoretically, such cracks and failures are expected due to the inherent characteristics of FRP bars, which exhibit relatively weak interlaminar shear resistance [10]. This weakness arises from the presence of unreinforced resin layers between fiber layers. Additionally, the low elastic modulus of BFRP bars further contributes to the

development of these crack failures. However, since BFRP bars are resistant to corrosion, the significance of crack width is lower compared to steel reinforcement.

### Deflections

STL-1 and STL-2 showed similar performance, failing at loads of 20 kN and 21.8 kN, with midspan deflections of 4.8 mm and 4.7 mm, respectively. In contrast, BFP-1 and BFP-2 exhibited greater load bearing capacity, with 26 kN and 30 kN and midspan deflections of 16.17 mm and 21.50 mm, respectively. Figure 7 below summarized the load and deflection relationships for each sample at midspan. The results indicate a significant increase in deflection in the concrete beams reinforced with BFRP bars, with the average deflection values of these two samples being three times higher than those of the two concrete beams reinforced with steel bars.

### Theoretical background

For a simply supported beam with a span of length ( $l$ ), subjected to two equal concentrated loads ( $P/2$ ) positioned symmetrically on either side of the beam centerline, the maximum deflection ( $\Delta_{max}$ ) occurring at the beam's center can be calculated using the following expression in (Equation 1).

$$\Delta_{max} = \frac{Px}{24E_cI_e} (3l^2 - 4x^2) \tag{1}$$

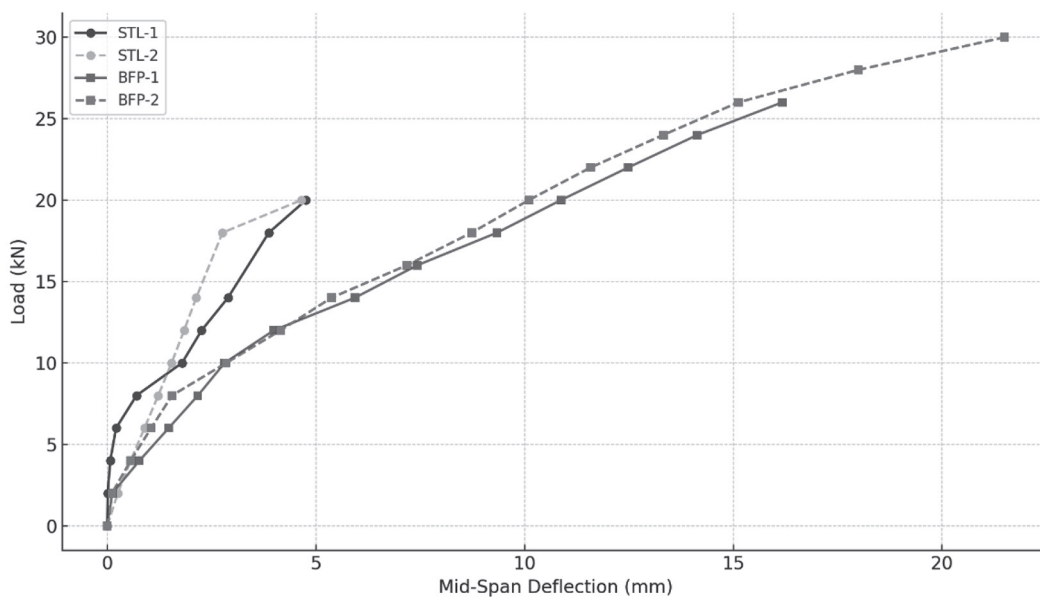


Figure 7. Load vs. deflection curves at midspan

where:  $x$  – the distance from the support to the point of load application,  $L$  – the total length of the beam,  $P$  – the applied load, and  $E_c$  – the modulus of elasticity of the concrete,  $I_{cr}$  – the moment of inertia of the cracked section, while the immediate deflection under service loads is determined using the effective moment of inertia  $I_e$ .

For the FRP reinforced beams, various scholars have proposed modifications to the formula for  $I_e$ . As per Bischoff [17], the effective moment of inertia, derived from curvature, is calculated as (Equation 2):

$$I_e = \frac{I_{cr}}{1 - \left( \frac{I_{cr}}{I_g} \right) \left( \frac{M_{cr}}{M_a} \right)^2} \quad (2)$$

where:  $M_a$  – is applied moment,  $I_g$  – is the gross sectional moment of inertia ( $bh^3/12$ ),  $M_{cr}$  – is a cracking moment calculated by  $2f_r I_g / h$ . where,  $f_r = 0.62 \sqrt{f_c'}$  and  $h$  – is depth of concrete beam, and  $I_{cr}$  – is the moment of inertia of the cracked section.

On the other hand, The ACI 318-08 [25] and Branson [26] propose the following equation (Equation 3) for the effective moment of inertia;

$$I_e = \left[ \frac{M_{cr}}{M_a} \right]^3 I_g + \left[ 1 - \left( \frac{M_{cr}}{M_a} \right)^3 \right] I_{cr} \quad (3)$$

Due to the substantially higher ratio of  $I_g/I_{cr}$  in the beams reinforced with BFRP, the deflection values computed using this formula are often underestimated. Yost et al. [27] introduced the Branson  $\beta_d$  expressed on (Equation 7) parameter to account for the bond between concrete and BFRP bars and the modulus of elasticity of BFRP bars. The modified effective moment of inertia is given by (Equation 4);

$$I_e = \left[ \frac{M_{cr}}{M_a} \right]^3 \beta_d I_g + \left[ 1 - \left( \frac{M_{cr}}{M_a} \right)^3 \right] I_{cr} \quad (4)$$

where:  $I_{cr}$  – is the moment of inertia of the cracked section which can be calculated by (Equation 5).

$$I_{cr} = \frac{bd^3}{3} k^3 + n_f A_f d^2 (1 - k)^2 \quad (5)$$

where:  $n_f = E_f/E_c$  – is the modular ratio of reinforcement to concrete and  $k$  – is the ratio of the depth of the neutral axis to the reinforcement depth calculated by (Equation 6);

$$k = \sqrt{2\rho_f n_f + (\rho_f n_f)^2} - \rho_f n_f \quad (6)$$

$$\beta_d = \alpha_b \left( \frac{E_f}{E_s} + 1 \right) \quad (7)$$

$$\alpha_b = 0.064 \left( \frac{\rho_f}{\rho_{fb}} \right) + 0.013 \quad (8)$$

The ACI 440.1R-06 [10] expression modifies Yost et al.'s [24] equation by revising the  $\beta_d$  (Equation 9) parameter as follows:

$$\beta_d = \frac{\rho_f}{5\rho_{fb}} \leq 1 \quad (9)$$

The theoretical deflections of the tested BFRP-reinforced and steel-reinforced beams were calculated using the procedures and formulas summarized in Table 4.

The following graph, (Figure 8) illustrates the comparison between average experimental deflections of the concrete beams reinforced with steel bars and BFRP bars with the different theoretical values of deflection described above.

During the initial stages of the loading phase, the experimental deflection values closely align with theoretical predictions. However, at higher

**Table 4.** Deflection calculations of beams with BFRP bars from different theories

Literature	Proposed equation for effective moment of inertia ( $I_e$ )
Bischoff [17]	$I_e = \frac{I_{cr}}{1 - \left( \frac{I_{cr}}{I_g} \right) \left( \frac{M_{cr}}{M_a} \right)^2}$
Branson [23]	$I_e = \left[ \frac{M_{cr}}{M_a} \right]^3 I_g + \left[ 1 - \left( \frac{M_{cr}}{M_a} \right)^3 \right] I_{cr}$
Yost et al. [24]	$I_e = \left[ \frac{M_{cr}}{M_a} \right]^3 \beta_d I_g + \left[ 1 - \left( \frac{M_{cr}}{M_a} \right)^3 \right] I_{cr}; \quad \beta_d = \alpha_b \left( \frac{E_f}{E_s} + 1 \right), \quad \alpha_b = 0.064 \left( \frac{\rho_f}{\rho_{fb}} \right) + 0.013$
ACI 440.1R-06 [10]	$I_e = \left[ \frac{M_{cr}}{M_a} \right]^3 \beta_d I_g + \left[ 1 - \left( \frac{M_{cr}}{M_a} \right)^3 \right] I_{cr}; \quad \beta_d = \frac{\rho_f}{5\rho_{fb}} \leq 1,$
Maximum deflection $\Delta_{max}$	
$\Delta_{max} = \frac{Px}{24E_c I_e} (3L^2 - 4x^2)$	

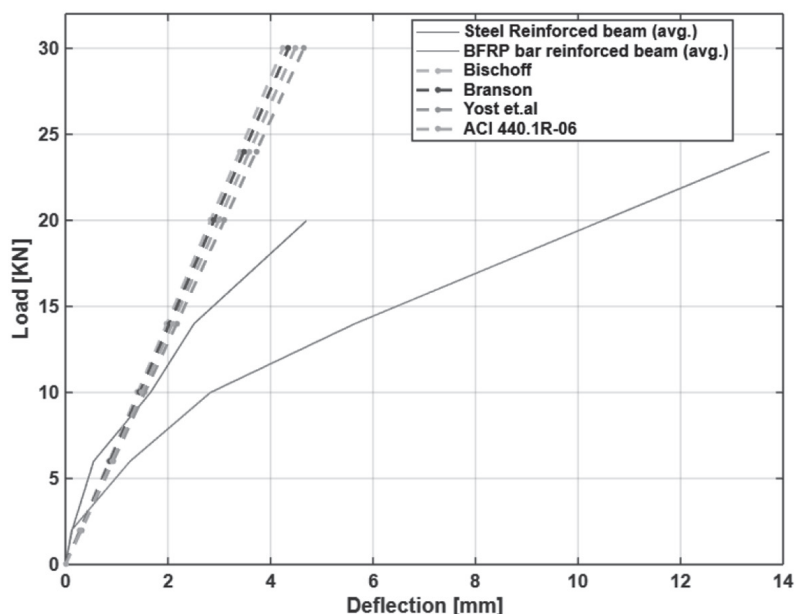


Figure 8. Load vs. deflection comparison of average experimental values and theoretical literatures

loads exceeding 10 kN, the tested samples, particularly the beams reinforced with BFRP bars, exhibit greater deflection than anticipated in theoretical estimations. This discrepancy suggests that additional mechanisms may be necessary to enhance the deflection resistance of such beams.

## CONCLUSIONS

The concrete beams reinforced with BFRP bars show enhanced load-bearing capacity compared to those reinforced with steel. The failure mode analysis indicates that the BFRP bar reinforced beams exhibit significant bending behavior before failure, whereas the steel reinforced concrete beams fail at an earlier stage. However, the BFRP bar-reinforced beams show signs of shear and bond failure, as evidenced by horizontal cracking near the supports. This behavior is attributed to the lower elastic modulus and other mechanical properties of BFRP bars. Despite the increased crack formation in the BFRP bar-reinforced beams, the inherent corrosion resistance of the bars allows for larger crack widths. Additionally, the comparison with theoretical models revealed variations in deflection predictions, emphasizing the need for refined analytical tools. The higher deflections observed in the case of BFRP bar-reinforced beams highlight the need for further research to optimize their structural performance.

## Acknowledgments

This research is funded by Bialystok University of Technology under project number WI/WB-IIL/9/2023.

## REFERENCES

- Ochshorn J. (2010). *Structural elements for architects and builders*. Butterworth-Heinemann (an imprint of Elsevier Press). <https://doi.org/10.1016/B978-1-85617-771-9.00003-9>
- Mahadev Desai (2018). *Pros and Cons of Steel Reinforcement Bars*. Available online: <https://gharpedia.com/blog/pros-and-cons-of-steel-reinforcement-bars/> (accessed on 11 November 2022).
- Deitz DH, Harik IE, Gesund H. (1999). One-way slabs reinforced with glass fiber reinforced polymer reinforcing bars. In: *ACI proceedings, the fourth international symposium*, Detroit; 279– 86. <https://trid.trb.org/View/638333>
- Alsayed SH, Al-Salloum YA, AlMusallam TH. (1997). Shear design for beams reinforced by GFRP bars. In: *Proceedings of the third international symposium on non-metallic (FRP) reinforcement for concrete structures (FRPRCS-3)*, Japan, 2; 285–92. <https://doi.org/10.1007/BF02480431>
- Belay Abel A., Julita Krassowska, and Marta Kosior-Kazberuk. (2024). Comparative performance analysis of small concrete beams reinforced with steel bars and non-metallic reinforcements *Applied Sciences* 14(10): 3957. <https://doi.org/10.3390/app14103957>

6. Nayal, HARR, Melhem H. 2003. Response prediction of concrete beams reinforced with FRP bars. *Composite Structures*, 65,193–204. <https://doi.org/10.1016/j.compstruct.2003.10.016>
7. Abdalla HA. (2002). Evaluation of deflection in concrete members reinforced with fiber reinforced polymer (FRP) bars. *Composite Structures*, 56, 63–71. [https://doi.org/10.1016/S0263-8223\(01\)00188-X](https://doi.org/10.1016/S0263-8223(01)00188-X)
8. Toutanji H, Deng Y. (2002). Deflection and Crack-width prediction of concrete beams reinforced with glass FRP rods. *Construction and Building Materials*, 17, 69–74. [https://doi.org/10.1016/S0950-0618\(02\)00094-6](https://doi.org/10.1016/S0950-0618(02)00094-6)
9. Michaluk CR, Rizkalla SH, Tadros G and Benmokrane B. (1998). Flexural behavior of one-way concrete slabs reinforced by fiber reinforced plastic reinforcements. *ACI structural Journal*, 95, 353–365. <https://trid.trb.org/View/487515>
10. ACI 440.1R-06; *Guide for the Design and Construction of Concrete Reinforced with FRP Bars*. ACI Committee 440. American Concrete Institute: Farmington Hills, MI, USA, 2006. Available online: <https://www.iranfrp.ir/wp-content/uploads/2018/12/13.pdf>
11. Gdoutos EE, Pilakoutas K, Rodopoulos CA. (2000). Failure Analysis of Industrial Composite Materials, McGraw-Hill Professional. [https://search.lib.utexas.edu/permalink/01UTAU\\_INST/vu6c1o/alma991037251059706011](https://search.lib.utexas.edu/permalink/01UTAU_INST/vu6c1o/alma991037251059706011)
12. Amran YM, et al. (2018). Properties and applications of FRP in strengthening RC structures: A review. *Structures, Elsevier*. <https://doi.org/10.1016/j.istruc.2018.09.008>
13. Reeve S. (2022). 5 reasons to use fiber-reinforced polymer (FRP). Available online: <https://www.creativecompositesgroup.com/blog/5-reasons-use-fiber-reinforced-polymer-frp> (accessed on 05 June 2023).
14. Urbanski M, Lapko A, Garbacz A. (2013). Investigation on concrete beams reinforced with basalt re-bars as an effective alternative of conventional R/C structures. *Procedia Eng.* 57, 1183–1191. <https://doi.org/10.1016/j.proeng.2013.04.149>
15. Krassowska, J., Ramírez, C.P. (2022). Flexural capacity of concrete beams with basalt fiber-reinforced polymer bars and stirrups. *Materials*, 15, 8270. <https://doi.org/10.3390/ma15228270>
16. Kosior-Kazberuk M, Krassowska J. (2019). Analysis of deflection and cracking of concrete beams with non-metallic reinforcement. *Syst. Saf. Hum.-Tech. Facil.-Environ.*, 1, 782–789. <https://doi.org/10.2478/czoto-2019-0100>
17. Bischoff PH. (2007). Deflection calculation of FRP reinforced concrete beams based on modifications to the existing Branson equation. *Journal of Composites for Construction*, 11(1), 4–14. [https://doi.org/10.1061/\(ASCE\)1090-0268\(2007\)11:1\(4\)](https://doi.org/10.1061/(ASCE)1090-0268(2007)11:1(4))
18. Ashour A. (2006). Flexural and shear capacities of concrete beams reinforced with GFRP bars. *Constr. Build. Mater.* 20, 1005–1015. <https://doi.org/10.1016/j.conbuildmat.2005.06.023>
19. Zhang Z et al. (2023). Research progress on short-term mechanical properties of FRP bars and FRP-reinforced concrete beams. *Journal of Traffic and Transportation Engineering*. <https://doi.org/10.1016/j.jtte.2023.06.005>
20. Li Q, et al. (2024). Behavior of geometrically-similar Basalt FRP bars-reinforced concrete beams under dynamic torsional loads. *Journal of Sandwich Structures & Materials*. <https://doi.org/10.1177/105678952412458>
21. Kumar P, et al. (2023). Experimental investigation of the effects of FRP bar fiber type and surface characteristics on the performance of reinforced concrete beams. *Iranian Journal of Science and Technology, Transactions of Civil Engineering*. <https://doi.org/10.1007/s40996-023-01301-9>
22. EN 12390-3:2009; Testing Hardened Concrete—Part 3, (2009): Compressive Strength of Test Specimens. European Committee for Standardization: Brussels, Belgium. Available online: [https://i2.saiglobal.com/mpc2v/preview/497200114258.pdf?sku=855939\\_SAIG\\_NSAI\\_NSAI\\_2751255&nsai\\_sku=i-s-en-12390-3-2019-855939\\_saig\\_nsai\\_nsai\\_2751255](https://i2.saiglobal.com/mpc2v/preview/497200114258.pdf?sku=855939_SAIG_NSAI_NSAI_2751255&nsai_sku=i-s-en-12390-3-2019-855939_saig_nsai_nsai_2751255) (accessed on 2 February 2024)
23. EN 12390-5:2019; Testing Hardened Concrete—Part 5 2019: *Flexural Strength of Test Specimens*. European Committee for Standardization: Brussels, Belgium. Available online: <https://cdn.standards.iteh.ai/sample/s/64401/9078b3193a544c26a16a278c66f0ae34/SIST-EN-12390-5-2019.pdf> (accessed on 2 February 2024).
24. EN 12390-13:2013; Testing Hardened Concrete. (2013). *Determination of Secant Modulus of Elasticity in Compression*. European Committee for Standardization: Brussels, Belgium. Available online: <https://knowledge.bsigroup.com/products/testing-hardened-concrete-determination-of-secant-modulus-of-elasticity-in-compression?version=standard> (accessed on 2 February 2024).
25. ACI Committee, 3. (2008). *Building code requirements for structural concrete (ACI 318-08) and commentary*. American Concrete Institute. Available online: [https://myyardimci.weebly.com/uploads/1/6/3/4/16347790/building\\_design\\_code\\_english.pdf](https://myyardimci.weebly.com/uploads/1/6/3/4/16347790/building_design_code_english.pdf)
26. Branson, D.E. (1977). *Deformation of concrete structures*. [https://www.semanticscholar.org/paper/Deformation-of-concrete-structures-Branson/dfd5e7f1cb2861cb921301661f2305cf088b8ce?utm\\_source=direct\\_link](https://www.semanticscholar.org/paper/Deformation-of-concrete-structures-Branson/dfd5e7f1cb2861cb921301661f2305cf088b8ce?utm_source=direct_link)
27. Yost, J.R., Gross, S.P. and Dinehart, D.W., 2003. Effective moment of inertia for glass fiber-reinforced polymer-reinforced concrete beams. *Structural Journal*, 100(6), 732–739. <https://doi.org/10.14359/12839>